TU Delft

Delft University of Technology

A Quasi-Analytical Tool for the Characterization of Transmission Lines at High Frequencies

Berkel, S. van; Garufo, A.; Llombart Juan, N.; Neto, Andrea

DOI
10.1109/MAP.2016.2541617

Publication date
2016

Document Version
Accepted author manuscript

Published in
IEEE Antennas and Propagation Magazine

Citation (APA)
Berkel, S. V., Garufo, A., Llombart Juan, N., & Neto, A. (2016). A Quasi-Analytical Tool for the Characterization of Transmission Lines at High Frequencies. *IEEE Antennas and Propagation Magazine*, *58*(3), 82-90. https://doi.org/10.1109/MAP.2016.2541617

Important note
To cite this publication, please use the final published version (if applicable).
Please check the document version above.

Copyright
Other than for strictly personal use, it is not permitted to download, forward or distribute the text or part of it, without the consent of the author(s) and/or copyright holder(s), unless the work is under an open content license such as Creative Commons.

Takedown policy
Please contact us and provide details if you believe this document breaches copyrights.
We will remove access to the work immediately and investigate your claim.

This work is downloaded from Delft University of Technology.
For technical reasons the number of authors shown on this cover page is limited to a maximum of 10.

A Quasi-Analytical Tool for the Characterization of Transmission Lines at High Frequencies

Sven L. van Berkel, Alessandro Garufo, Nuria Llombart, and Andrea Neto

EDITOR'S NOTE

High-frequency transmission lines bring a variety of challenges, both practical and theoretical. Regarding the latter, quasi-static approaches are generally of limited use because one has to deal with a variety of full-wave effects. This issue's "EM Programmer's Notebook" column provides a review of the issues that must be addressed and presents a publicly available software tool.

In this article, we present a freely accessible software tool that allows for fast characterization of dynamic phenomena in a wide variety of transmission lines that include characteristic impedance, effective dielectric constant, and losses, such as radiation into space and surface waves. For printed transmission lines, the radiation effects are of particular importance when the transverse dimensions of the transmission lines become significant in terms of wavelength. Generally, dispersion and losses of the line due to these dynamic phenomena are predicted by full-wave simulations as quasi-static formula do not suffice. The presented software tool, freely downloaded from http://terahertz.tudelft.nl, is capable of accurately analyzing the most widely used transmission lines at high frequencies.

At low frequencies, for example, in the case of printed transmission lines below ~50 GHz, the main parameters of a transmission line, such as the propagation constant, characteristic impedance, and attenuation constant, can generally be approximated using quasi-static formulations [1]. However, when the transverse dimensions of the transmission lines become significant in terms of the wavelength ($\sim\lambda/20$), dynamic phenomena in the line become nonnegligible and can have a significant influence on these parameters. The excitation of leaky higher-order modes causes radiation into space and surface waves, which launches power within the stratification [2], [3]. In fact, multiple modes can propagate simultaneously in the transmission line [4]. These phenomena could be avoided with micrometric integrated technology. However, one may wish to still use low-cost printed circuit board technology while minimizing the effects of these higher-order modes. For example, a coplanar waveguide (CPW), with a 100-μm minimum feasible dimension in width and spacing (see Figure 1), will radiate while excited in its differential propagation mode at higher frequencies ($f \geq 50$ GHz). Moreover, these effects will also be present in integrated technology circuits operating in the submillimeter-wavelength range. Therefore, it is of importance to characterize the

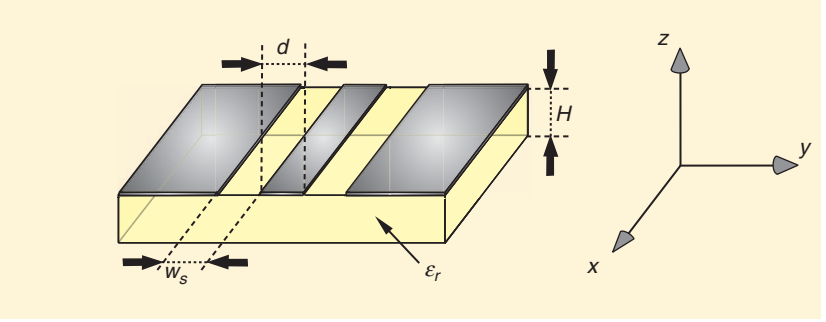

FIGURE 1. An example of a transmission line (CPW) with its reference axis. w_s is the width of the slot (or strip for strip-type structures), d is the spacing between multiple lines, and H and ϵ_r are the height and the relative permittivity of the dielectric slab, respectively.

impact of these dynamic effects. To date, there are no (quasi)analytical tools for estimating radiation losses. In addition, equivalent formulas for coplanar transmission line surface-wave losses [2] are not applicable for more complex structures dealing with an arbitrary stratification or superconductivity. A designer willing to perform a detailed analysis will be obliged to resort to the use of full-wave simulations that are very time consuming and require expensive licenses.

For this purpose, a freely available software tool (Figure 2) has been developed that can characterize transmission lines at high frequencies. This tool is based on a fast quasi-analytical model that is more extensively described in [5]–[8].

We present a freely accessible software tool that allows for fast characterization of dynamic phenomena in a wide variety of transmission lines.

QUASI-ANALYTICAL MODEL

The tool follows a quasi-analytical approach that makes use of transmission line formalism [6]–[8]. This formalism derives the Green's functions (GFs) of the transmission line by solving the pertinent integral equation of infinite line currents radiating in the presence of stratified media, excited by a Δ gap (Figure 3). In the software tool, four possible layers of stratification are considered:

1) an infinite top medium
2) a finite upper slab
3) a finite lower slab
4) an infinite bottom medium.

With this choice of stratification, most commonly used printed transmission lines can be modeled having a different number of conductors (e.g., see Figure 1).

TRANSMISSION LINE FORMALISM

In the setup of the problem, the transmission line is composed of n guiding structures (strips/slots), e.g., $n = 1$ for a microstrip and $n = 2$ for a CPW. The transmission line is assumed to be oriented along $\hat{x}$, the conductors are infinitesimal in thickness, and the stratification is homogeneous in the $(\hat{x}, \hat{y})$ plane. The transmission line formalism is constructed by first defining two types of integral equations: the electric field integral equation (EFIE) for strips in [6] and [7] or the continuity of magnetic field integral equation (CMFIE) for slots in [8]. In this formulation, the electric (magnetic) fields are averaged over the width of the strip (slot). The unknown equivalent electric (magnetic) current distributions along the lines $\underline{c}_{eq}(x, y)$, are assumed to be separable in space dependency [5]: $c^i_{eq}(x, y) = c_i(x) \cdot c_t(y - id_y)$ for $i = 0$: $n-1$, where $d_y = d + w_s$ is the spacing between the centers of the coplanar lines (Figure 1). The width of the line is assumed to be much smaller than the wavelength $w_s \ll \lambda$, which allows for characterizing the transverse dependence $c_t(y)$ by the quasi-static edge singularities:

$$c_t(y) = \frac{2}{w_s \pi} \frac{1}{\sqrt{1 - \left(\frac{2y}{w_s}\right)^2}} \text{ for } |y| < w_s.$$

In this way, $\underline{c}(x)$ represents the longitudinal electric currents (voltage drop) along the strips (slots).

After representing the pertinent integral equations in the spectral domain and equating the integrands, the longitudinal electric or magnetic currents $\underline{c}(x)$ along the transmission line can be expressed as an inverse Fourier transform of the current spectrum in the longitudinal domain of the lines (1). This formulation is known as *transmission line formalism*:

$$\begin{aligned} c(x) &= \frac{1}{2\pi} \int_{-\infty}^{\infty} \underline{\underline{D}}^{-1}(k_x) \underline{N}_0 \\ &\quad \times \sin c\left(\frac{k_x \Delta}{2}\right) e^{-jk_x x} dk_x \\ &= \frac{1}{2\pi} \int_{-\infty}^{\infty} \frac{\underline{\underline{A}}(k_x)}{\det(\underline{\underline{D}}(k_x))} \underline{N}_0 \\ &\quad \times \sin c\left(\frac{k_x \Delta}{2}\right) e^{-jk_x x} dk_x, \end{aligned} \quad (1)$$

where $\underline{\underline{A}}(k_x)$ is the adjugate of $\underline{\underline{D}}(k_x)$. For the EFIE (CMFIE), the denominator $\underline{\underline{D}}(k_x)$ represents the average transverse electric (magnetic) field radiated on the strip (slot) by the equivalent

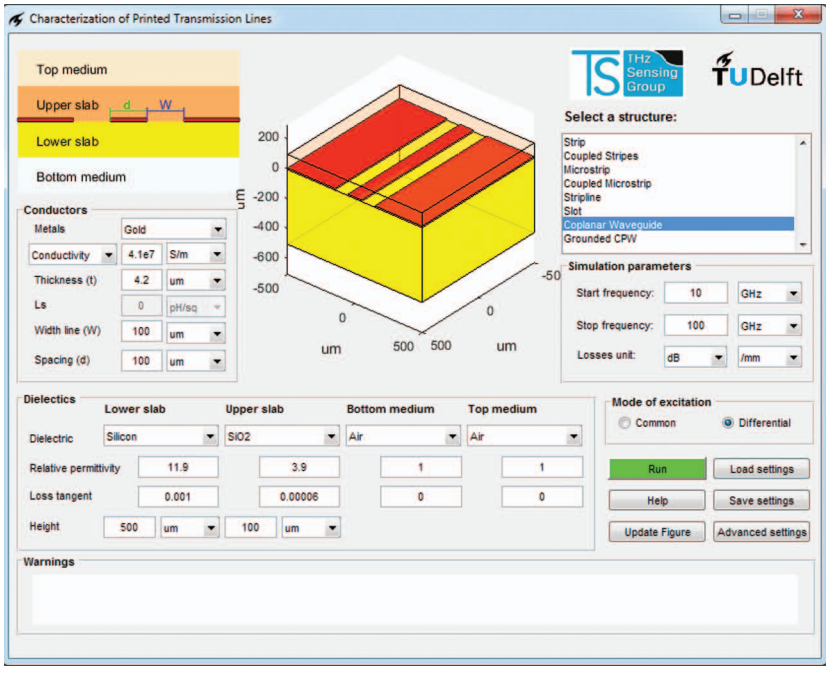

FIGURE 2. The GUI of the software tool using the presented quasi-analytical model. The most commonly used printed transmission lines, with user-defined stratification, can be simulated.

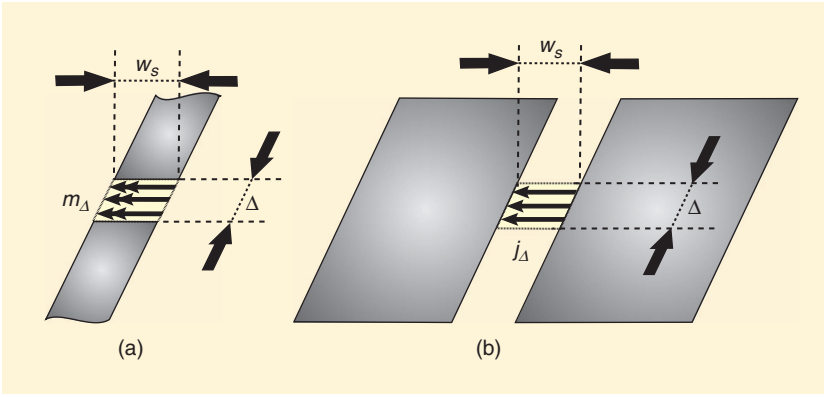

FIGURE 3. The Δ-gap excitation for (a) strip-type and (b) slot-type transmission lines, a magnetic dipole $m_\Delta(x, y)$, and an electric dipole $j_\Delta(x, y)$.

currents. The excitation law $\underline{N}_0$ of the magnetic (electric) dipole sources in the Δ gap (Figure 3) must ensure that the transmission line is fed by 1 V (1 A) in the case of strips (slots). This implies that the amplitude of the excitations $|N_{0,i+1}| = 1/n$ (V or A) for $i = 0{:}n{-}1$. Moreover, $\underline{N}_0$ has to select any propagation modes (e.g., common or differential excitation) for transmission lines composed of $n > 1$ guiding structures, e.g., for a CPW excited in its differential propagating mode $\underline{N}_0 = [0.5 - 0.5]$ A. The denominator $\underline{\underline{D}}(k_x)$ can, in turn, be expressed as a transverse spectral integration (2):

$$D_{n,i+1}(k_x) = \frac{1}{2\pi}\int_{-\infty}^{\infty} G_{xx}^{F,C}(k_x,k_y)\,C_t(k_y) \times e^{-jk_y(n-i)d_y}\,dk_y \qquad (2)$$

for $i = 0{:}n{-}1$. In (2), $G_{xx}^{F,C}(k_x, k_y)$ is the spectral GF of the corresponding stratification in the absence of the guiding structure: $G_{xx}^{E,J}(k_x, k_y)$ for strip-type and $G_{xx}^{H,M}(k_x, k_y)$ for slot-type transmission lines. The GF of this stratification can be modeled as planar stratified media [9]. The assumed edge singular distribution $c_t(y)$ has an analytic Fourier transform

$$J_0\left(\frac{k_y w_s}{2}\right).$$

The averaging of the fields over the width of the strips (slots) leads to a sinc-function multiplication of the transverse current distribution:

$$C_t(k_y) = J_0\left(\frac{k_y w_s}{2}\right)\operatorname{sinc}\left(\frac{k_y w_s}{2}\right).$$

The exponential term in (2) accounts for the coupling between multiple lines.

INTEGRATION PATH

The result of the integration in k_x from $-\infty$ to $+\infty$ in the inverse Fourier transform (1) depends mostly on the polar singularities in $\underline{\underline{D}}^{-1}(k_x)$. The procedure of finding these polar singularities is based on solving $\det(\underline{\underline{D}}(k_x)) = 0$, which defines the dispersion equation. These singularities are associated with the propagating modes along the transmission line. Three characteristic propagating modes are of interest:

1) bounded modes: nonradiative modes such as the main propagating mode in a microstrip
2) surface-wave modes: propagating modes exciting a surface wave intrinsic to the stratification
3) leaky-wave modes: propagating modes radiating in a dense infinite medium, as in the case of circuits placed at the bottom of a dielectric lens.

To evaluate the singularities of $\underline{\underline{D}}(k_x)$, the integration in the transverse spectral domain (2) must be performed numerically. However, the choice of the transverse integration path in k_y is nontrivial because it depends on the location of the propagating mode in the longitudinal k_x domain. When an infinite stratification is present, branch cuts will appear in the spectrum, leading to different Riemann sheets. Changing the integration path into the different Riemann sheets allows for finding not only bounded modes but also leaky modes. The integration path of the bounded- and surface-wave mode for a microstrip has been extensively studied by Mesa [6], [7], and a leaky-wave mode of a slotline has been studied by Neto [8]. In choosing the integration path, care has to be taken in guaranteeing that the solutions of the dispersion equation are actually physically valid propagating modes. For example, when a surface-wave pole is present and excited, this pole should be enclosed by the transverse integration path. A surface-wave pole is excited when $\beta_{\text{mode}} < \beta_{\text{SFW}}$ [2], where β_{mode} and β_{SFW} are the phase constants of the main propagating mode and the surface-wave pole, respectively. In addition, when the main propagating mode is in fact a leaky-wave mode, the transverse integration path in (2) should cross branch cuts to integrate over the bottom Riemann sheet, where the leaky-wave pole can be found.

To date, there are no (quasi) analytical tools for estimating radiation losses.

Using the software tool, the height of the stratification is limited such that only one mode will propagate in the transmission line. The tool will automatically select the appropriate integration path associated with this specific type of propagating mode.

TRANSMISSION LINE CHARACTERISTICS

Using the quasi-analytical model described in the previous section, numerous interesting characteristics of transmission lines can be analyzed. The model is used to generate a software tool that is made freely accessible and capable of analyzing the most widely used printed transmission lines. The graphical user interface (GUI) is shown in Figure 2. The user can select the materials and loss tangents of four possible layers of stratification: two finite dielectric slabs and two infinite media. Conductor and dielectric losses in the structure are described by supplying a value for

a finite conductivity and loss tangent, respectively. The tool can characterize radiation losses, and it takes account of the first surface wave appearing in the stratification. The output of the tool is composed of four values, as can be seen in Figure 4:

- the complex normalized wavenumber
- the effective dielectric constant
- the characteristic impedance
- losses.

This section describes the implementation and validation of these transmission line characteristics in the discussed quasi-analytical model. The transverse dimensions w_s and d of the structures to be validated are generally chosen to be the minimum transverse dimensions typically possible for printed circuit board technology, i.e., 100-μm strip (slot) width and 127-μm dielectric slab height. A CPW will be excited with a Δ-gap excitation in the differential mode.

The tool solves the dispersion equation by using a Taylor series expansion around an initial guess point k_{init} for the propagation constant along the line. This leads to a first-order approximation of the propagation constant associated to the main mode (3):

$$k_{\text{mode}} \approx k_{\text{init}} - \frac{\det(\underline{\underline{D}}(k_{\text{init}}))}{\det(\underline{\underline{D}}(k_{\text{init}}))'}. \quad (3)$$

For n coplanar lines, the dispersion equation will have n solutions, corresponding to the number of supported propagating modes along the line. The tool allows for selecting the propagating mode of interest (e.g., differential or common modes in a CPW). The first-order Taylor expansion is repeated by the algorithm until the achievement of a convergence goal that can be specified by the user. The resulting normalized complex wavenumber k/k_0, with $k = \beta - j\alpha$ and k_0 the free-space wavenumber, gives information regarding the dispersion of the transmission line and the losses associated with it.

The capability of characterizing this dispersion and losses is one of the significant advantages of using the presented quasi-analytical model. Losses due to radiation into space and surface waves in transmission lines with multiple and arbitrary layers of stratification can be easily investigated. In the remaining part of this section, the main parameters of a printed transmission line are investigated and validated when such dynamic phenomena are present and quasi-static formula often do not suffice. In these cases, the designer wishing to estimate these phenomena is generally required to resort to the use of full-wave simulations. In the presented validation, losses due to radiation into space and surface waves are studied, as well as ohmic losses in the conductors or stratification and the use of superconductors.

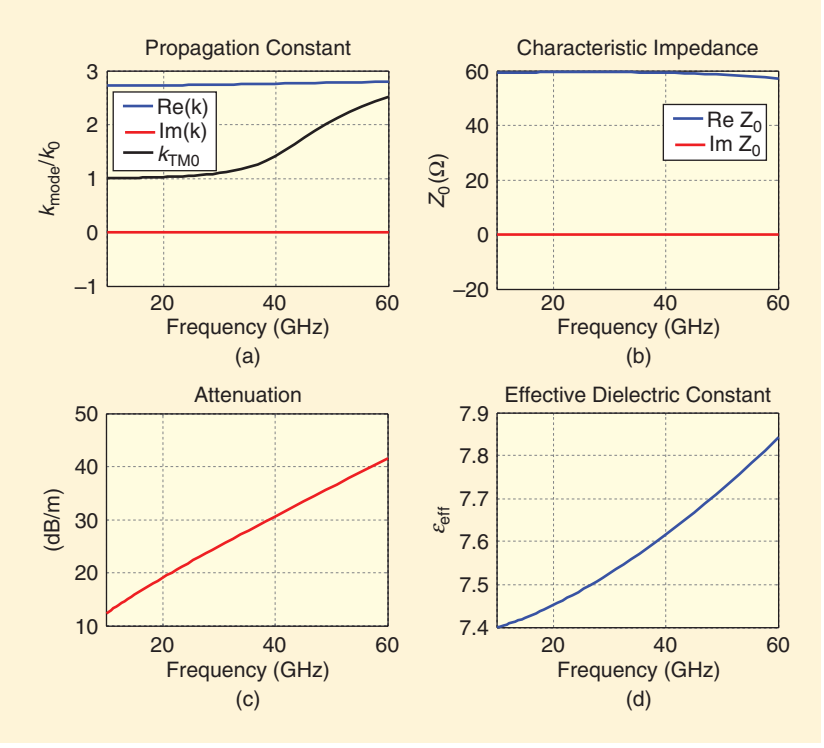

FIGURE 4. The output of the software tool: (a) complex wave number, (b) characteristic impedance of the main propagating mode, (c) losses (a superposition of ohmic and radiative losses), and (d) effective dielectric constant.

Losses due to radiation into space and surface waves in transmission lines with multiple and arbitrary layers of stratification can be easily investigated.

PHASE CONSTANT

The real part of the complex wavenumber β is the phase constant of the main propagating mode. The phase constant allows for calculating the effective dielectric constant of the transmission line

$$\epsilon_{r,\text{eff}} = \left(\frac{\beta}{\beta_0}\right)^2.$$

In Figure 5, one can see the real part of the complex normalized wavenumber (β/β_0), for a microstrip with $w_s = 100\,\mu$m, $H = 127\,\mu$m, and $\epsilon_r = 11.9$. Also shown is a CPW with $w_s = 100\,\mu$m, $d = 100\,\mu$m, $H = \infty$, and $\epsilon_r = 11.9$. The presented results are validated with full-wave simulations done in CST, where the main line parameters are extracted from the field distribution along the strip and slots.

ATTENUATION CONSTANT

The imaginary part of the wavenumber α is the superposition of attenuation due to conductor, dielectric, and radiative losses. These radiation losses can

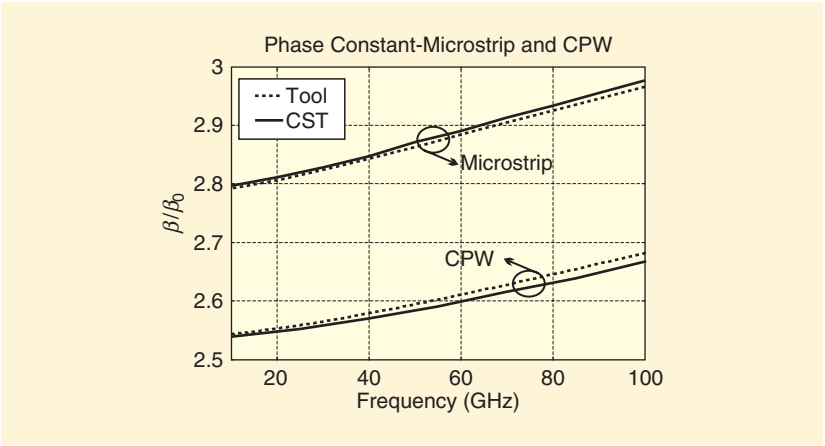

FIGURE 5. The output of the proposed tool for the real part (β/β_0) of the complex normalized wavenumber for a microstrip with $w_s = 100\,\mu$m, $H = 127\,\mu$m, and $\epsilon_r = 11.9$, and a CPW with $w_s = 100\,\mu$m, $d = 100\,\mu$m, $H = \infty$, and $\epsilon_r = 11.9$. The result is validated with full-wave CST simulations.

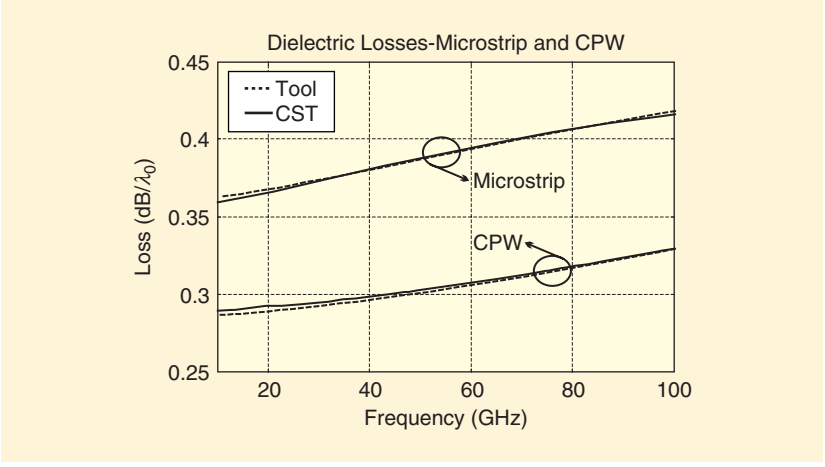

FIGURE 6. Dielectric losses for a microstrip and a CPW with $w_s = 100\,\mu$m, $d = 100\,\mu$m, $H = 127\,\mu$m, and $\epsilon_r = 11.9$. The dielectrics are characterized with a loss tangent of $\tan(\delta) = 0.005$. The result is validated with CST.

be due to excitation of an intrinsic surface wave or direct radiation into a dense infinite medium such as a silicon lens. The attenuation constant α, in nepers, can be converted to a loss figure, e.g., in dB/λ_{eff}, where

$$\lambda_{\text{eff}} = \frac{c}{f\sqrt{\epsilon_{r,\text{eff}}}}$$

is the effective wavelength of the main propagating mode.

DIELECTRIC LOSSES

Besides conductor losses, transmission lines can suffer from dielectric losses. These losses can be defined in the tool by means of a dielectric loss tangent $\tan(\delta)$. This loss tangent is implemented in the GF of the stratified media by defining the dielectrics with a complex relative permittivity (4):

$$\epsilon_{\text{lossy}} = \epsilon_0\epsilon_r(1 - j\tan(\delta)). \tag{4}$$

The dielectric losses for a microstrip and CPW are validated with $w_s = 100\,\mu$m, $d = 100\,\mu$m, $H = 127\,\mu$m, and $\epsilon_r = 11.9$. The dielectric slabs are characterized with a loss tangent of $\tan\delta = 0.005$. The results are shown in Figure 6 and are validated with CST.

CONDUCTOR LOSSES

Using the software tool, conductors are modeled to be infinitesimal. However, a change in surface impedance due to the finiteness of the conductor is implemented using the surface-impedance given in (5) [10]:

$$Z_s = \frac{R_{\text{RF}}}{1 - e^{-\frac{R_{\text{RF}}}{R_{\text{DC}}}}}, \tag{5}$$

where

$$R_{\text{DC}} = \frac{1}{\sigma t}$$

and

$$R_{\text{RF}} = (1+j)\sqrt{\frac{\pi\mu_0 f}{\sigma}}$$

with thickness t, conductivity σ, and free-space permeability μ_0. Ohmic losses in ground planes for both slot- and strip-type transmission lines can be easily implemented in the GF of the stratified media using a load that is equal to the high-frequency surface impedance $Z_{\text{gnd}} = R_{\text{RF}}$. The conductor losses for the main conductor of a strip-type transmission line are accounted for by means of a surface impedance boundary condition; imposing the EFIE on a lossy conductor gives rise to a nonzero tangential total electric field contribution. The total electric field $\underline{e}_{\text{tot}}$ can be related to the strip's surface impedance and current along the line: $\underline{e}_{\text{tot}} = Z_{\text{strip}}(y)\,\underline{c}_{\text{eq}}(x, y)$. It makes sense to define $Z_{\text{strip}}(y)$ as a function of the surface impedance Z_s. Proceeding as described in [10] and [11], accounting for the ohmic losses in the metal leads to a new denominator for the strip (6):

$$\underline{\underline{D}}_{\text{lossy}}(\underline{k}_x) = \underline{\underline{D}}(\underline{k}_x) + \frac{2}{w_s\pi}Z_s\,\underline{\underline{I}}. \tag{6}$$

In (6), $\underline{\underline{I}}$ is the identity matrix. The factor $2/w_s\pi$ accounts for the transverse edge singular current distribution [11]. Because the conductors are modeled to be infinitesimal, the electric current in the EFIE flowing on the top of the conductor is considered to be equal to the current flowing on the bottom of the conductor. However, for a microstrip on top of a dense dielectric slab, the current will mainly flow on the bottom of the conductor. This will have its influence on the effective surface impedance of the conductor. This current ratio can be approximated by making an assumption of the change in field

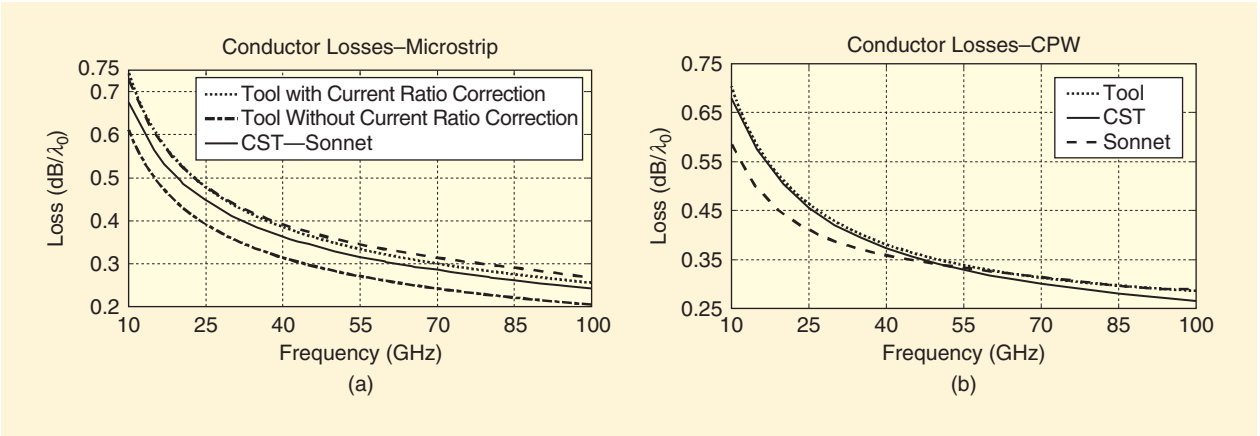

FIGURE 7. Conductor losses for (a) a microstrip and (b) a CPW with $w_s = 100\,\mu$m, $d = 100\,\mu$m, $H = 127\,\mu$m, $\epsilon_r = 11.9$, $t = 6\,\mu$m, and $\sigma = 4.1{\cdot}10^7$ S/m. For the microstrip, both the main conductor and the ground plane have a finite conductivity. The results are validated with CST and Sonnet.

distribution using the phase constant of the propagating mode:

$$r_j = 2\frac{\beta_{\text{mode}}}{(\beta_1 + \beta_2)},$$

where β_1 and β_2 are the phase constants of the adjacent media. The current ratio r_j is then used to define an equivalent high-frequency resistance $R'_{\text{RF}} = r_j R_{\text{RF}}$ [10].

For slot-type transmission lines, because the IE is different, the conductor losses can be calculated by following the approach proposed in [12]. The approach is based on applying the equivalence principle on the slot region by replacing the slot region with the same lossy conductor as that of the ground planes. The lossy conductor can then be implemented in the GF of the stratified media by means of an impedance characterized by $2Z_{\text{gnd}}$, in series with the stratification. The factor of two used arises here because in the tool, only the equivalent magnetic current is modeled, whereas in [12] the equivalent electric current is also included.

The conductor losses of a microstrip [Figure 7(a)] and a CPW [Figure 7(b)] are validated with $w_s = 100\,\mu$m, $d = 100\,\mu$m, $H = 127\,\mu$m, $\epsilon_r = 11.9$, $t = 6\,\mu$m and $\sigma = 4.1 \cdot 10^7$ S/m. For the microstrip, both the main conductor and ground plane are nonperfect. In (a), both results are shown for the case in which we neglect ($r_j = 1$) and the case in which we account for the influence of the asymmetric current magnitude on the top and bottom of the main conductor. For the CPW, a good match with full-wave simulations is provided. Because the different magnitude of magnetic currents is already accounted for in the GFs of the stratified media, no additional compensation factor is needed, as it is in the strip case.

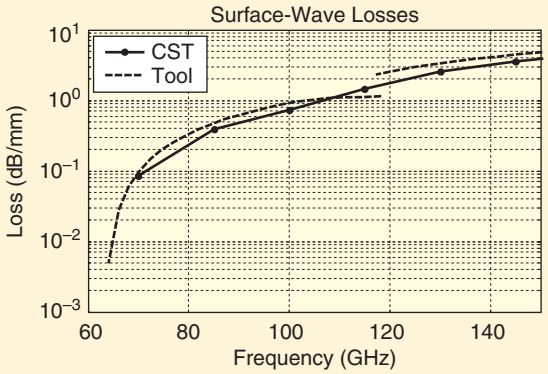

FIGURE 8. Losses associated with the excitation of the first two surface-waves (TM_0 and TE_1) for a CPW with $w_s = 100\,\mu$m, $d = 100\,\mu$m, $H = 500\,\mu$m, and $\epsilon_r = 11.9$. The result is validated with a full-wave CST simulation.

SURFACE-WAVE EXCITATION LOSSES

When the substrate height of a printed transmission line becomes larger than $\lambda/4$, the stratification will support an intrinsic surface wave. As the frequency increases, this surface wave can be excited by the main propagating mode along the transmission line (i.e., when $\beta_{\text{mode}} < \beta_{\text{SFW}}$ [2]). At this point, the software tool encloses the surface-wave poles in the integration path in the transverse domain, and the wavenumber becomes complex because the imaginary part is now associated with surface-wave losses.

The losses due to excitation of the TM_0 and TE_1 surface waves for a CPW with $w_s = 100\,\mu$m, $d = 100\,\mu$m, $H = 500\,\mu$m, and $\epsilon_r = 11.9$ are shown in Figure 8. It can be seen that at approximately 65 GHz, the surface-wave condition is verified, and the TM_0 surface wave is excited. Additionally, at approximately 118 GHz, the TE_1 surface wave will be excited.

RADIATION LOSSES

A CPW in the presence of an infinite dielectric half-space, simulating a silicon

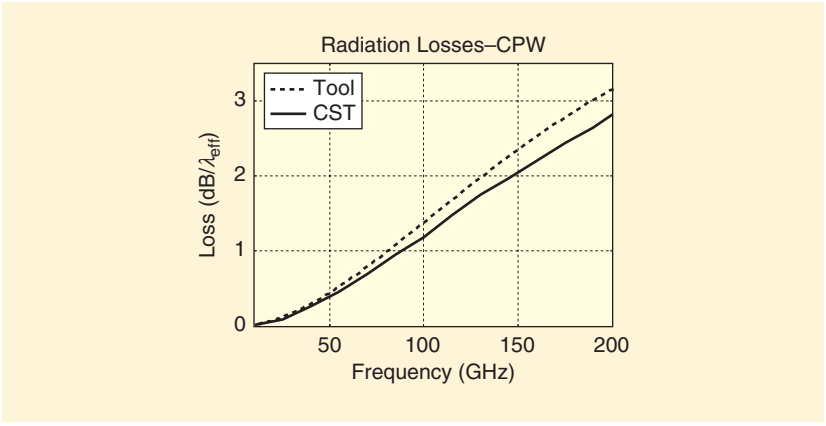

FIGURE 9. The radiation loss for a CPW with $w_s = 100\,\mu$m, $d = 100\,\mu$m, $H = \infty$, and $\epsilon_r = 11.9$. The result is validated with a full-wave CST simulation.

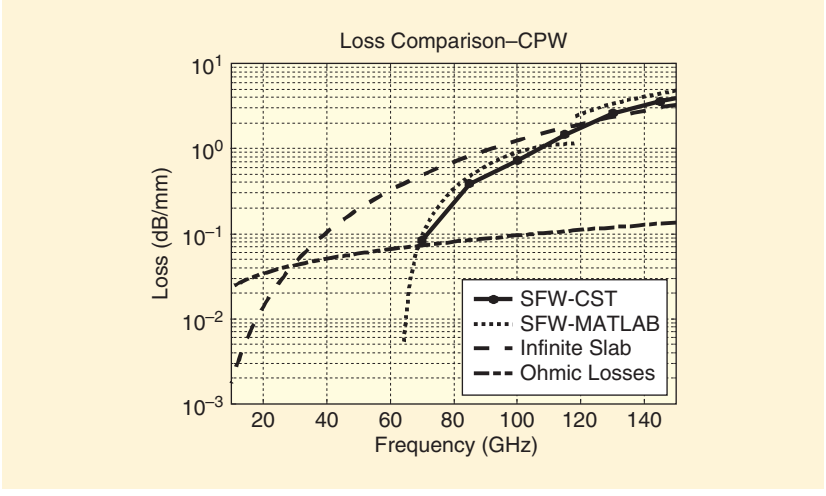

FIGURE 10. The loss comparison between a CPW printed onto a finite ($H = 500\,\mu$m) and infinite ($H = \infty$) dielectric slab with $w_s = 100\,\mu$m, $d = 100\,\mu$m, and $\epsilon_r = 11.9$. In addition, ohmic losses are calculated wherein the conductors have a finite conductivity of $\sigma = 4.1{\cdot}10^7$ S/m and thickness $t = 6\,\mu$m.

The software tool also provides the imaginary part of the characteristic impedance when the investigated lines support significant radiative losses.

lens, is investigated with dimensions $w_s = 100\,\mu$m, $d = 100\,\mu$m, $H = \infty$, and $\epsilon_r = 11.9$. The high-density dielectric lens above the CPW results in significant radiation of power in the lens, which can be characterized by the software tool. Because the dominant mode is a leaky-wave pole, the integration path in the transverse domain is required to cross the branch cuts to integrate over the bottom Riemann sheet. The output of the software tool is shown in Figure 9. It can be seen that at 200 GHz, approximately half of the power is radiated into the silicon after a propagation distance of λ_{eff}.

SURFACE-WAVE LOSS APPROXIMATION

The surface-wave losses in a CPW can be compared with radiation losses of a CPW into an infinite medium; this comparison is shown in Figure 10. As a reference, conductor losses are also calculated, wherein the conductors have a finite conductivity of $\sigma = 4.1{\cdot}10^7$ S/m and a finite thickness of $t = 6\,\mu$m. Analyzing Figure 10, it is clear that when the surface wave is excited, the losses are soon comparable to those due to direct radiation in the infinite dielectric. This is also verified using full-wave CST simulations. When a dielectric slab is larger than $\lambda_d/2$ in height, the medium can therefore also be modeled as an infinite dielectric. For this reason, the software tool restricts the height of a dielectric slab to an electrical height of $\lambda_d/2$, so that what is accounted for is only a first surface wave appearing in the stratification.

CHARACTERISTIC IMPEDANCE

A last important aspect in the characterization of transmission line is determining the characteristic impedance of the line. The characteristic impedance (admittance) of slot (strip)-type transmission lines can be calculated using the residue of the pole associated with the main propagating mode along the transmission line (7) [13]:

$$\underline{Z}_0^{\text{Slot}}/\underline{Y}_0^{\text{Strip}} = -j\frac{\underline{\underline{A}}(k_{\text{mode}})\,\underline{N}_0}{\det(\underline{\underline{D}}(k_{\text{mode}}))'}. \quad (7)$$

For coplanar lines excited in differential or common excitation mode, (7) is a vector from where the first element can be taken as the characteristic impedance. The characteristic impedance of a microstrip with $w_s = 100\,\mu$m, $H = 127\,\mu$m, and $\epsilon_r = 11.9$ is shown in Figure 11. For leaky lines suffering from losses due to radiation or surface-wave excitation, the definition in (7) can still be used, introducing an imaginary part on the characteristic impedance. Interested readers are referred to [14], in which a validation is given because the use of a complex propagation constant is not standard.

SUPERCONDUCTIVITY

In the software tool, the superconductive phenomenon is also implemented by describing a conductor with a kinetic inductance. This makes the tool suitable for characterizing more complex structures such as superconductive feeding networks or resonators in several types

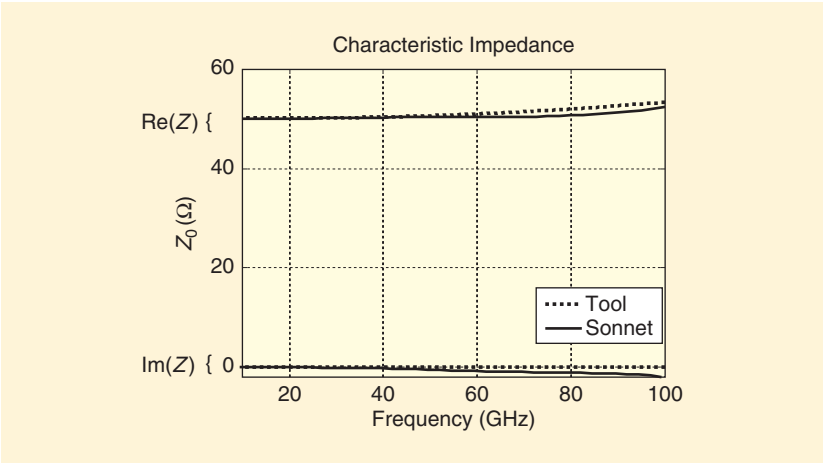

FIGURE 11. The characteristic impedance for a microstrip with $w_s = 100\ \mu$m, $H = 127\ \mu$m, and $\epsilon_r = 11.9$. The characteristic impedance is calculated using (7).

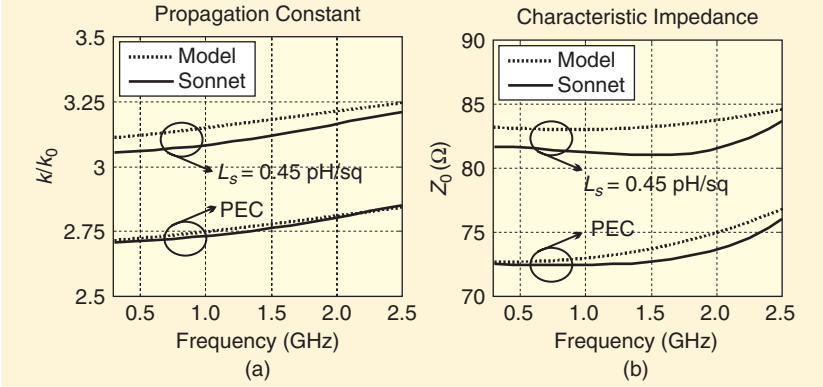

FIGURE 12. The effect of using a superconductor with $L_s = 0.45$ pH/sq is investigated in the (a) propagation constant and (b) characteristic impedance of a microstrip with $w_s = 1.5\ \mu$m, $H = 5\ \mu$m, and $\epsilon_r = 11.9$. The results are validated with Sonnet.

of terahertz detectors, e.g., transition edge sensors [15] or kinetic inductance detectors [16]. The total current flowing on the superconductor is the superposition of a current exhibiting normal losses and a lossless superconductive current. This assumption is referred to as the *two-fluid model* [17]. The software tool uses a simplified model, wherein the superconductors can be characterized via a complex conductivity $\sigma = \sigma_1 + j\sigma_2$ [18]. The real part of the complex conductivity σ_1 represents the normal fluid conductivity and the imaginary part σ_2 represents the super fluid conductivity. The complex conductivity is introduced in Z_s as is studied in [19]. The surface impedance Z_s used for the impedance boundary condition for a superconductor at low temperature ($\sigma_1 \ll \sigma_2$) can be characterized by $Z_s = R_s + jX_s$, where the surface resistance can be calculated by

$$R_s = \frac{1}{\lambda_L}\frac{\sigma_1}{2\sigma_2^2}$$

and $X_s = \omega\mu_0\lambda_L = \omega L_s$. λ_L is the London penetration depth, which is related to σ_2:

$$\lambda_L = \frac{1}{\sqrt{\mu_0\sigma_2\omega}}.$$

In the software tool, the surface impedance can be given by providing a value for the kinetic sheet inductance L_s and the real part of the conductivity.

As an example, we study the effect of superconductivity on the characteristic impedance and propagation constant of a microstrip with $w_s = 1.5\,\mu$m, $H = 5\,\mu$m, and $\epsilon_r = 11.9$. The conductors are considered to be NbTiN with a sheet inductance of $L_s = 0.45$ pH/sq. The comparison is shown in Figure 12. It is clear that using a superconductive material can have a significant influence on the characteristic impedance of a transmission line as well the propagation constant. No analytical or equivalent formulas can estimate these effects on the propagation constant and characteristic impedance of a transmission line; one has to resort to using full-wave simulators.

CONCLUSIONS

To date, no analytical tools exist for the fast characterization of transmission lines in terms of both ohmic and radiative losses. For approximating these phenomena, a few equivalent formulas exist. However, they only cover a small subset of transmission lines. A front-end designer has to resort to full-wave simulations, which are time consuming and require expensive licenses. A software tool is proposed that allows for a quick evaluation of the losses and impedance matching. The quasi-analytical model used allows for the characterization of several interesting phenomena such as surface-wave excitation, radiation, and superconductivity.

The software tool follows a quasi-analytical approach that is based on transmission line formalism resulting from a spectral representation of the integral equations. Solving the dispersion equation produces a complex wavenumber of a specific propagating mode along the transmission line. The complex wavenumber gives information regarding the dispersion and losses of this mode traveling along the transmission line. Subsequently, the quasi-analytical model is tested by validating the transmission line characteristics with full-wave simulations. The tool also provides the imaginary part of the characteristic impedance when the investigated

lines support significant radiative losses. Interested readers are referred to [14] for a more thorough discussion on this complex characteristic impedance. As mentioned previously, the software tool is freely accessible from our group's website at http://terahertz.tudelft.nl/.

AUTHOR INFORMATION

Sven L. van Berkel (s.l.vanberkel@tudelft.nl) received his B.S. and M.S. degrees in electrical engineering from the Delft University of Technology (TU Delft), The Netherlands, in 2012 and 2015, respectively. He is working toward his Ph.D. degree in the Terahertz Sensing Group, Department of Microelectronics, TU Delft. His research interests include passive imaging systems, ultrawideband antennas, and analytical/numerical methods for transmission line characterization. He is a Student Member of the IEEE.

Alessandro Garufo (A.Garufo@tudelft.nl) received his M.S. degree in telecommunications engineering from the University of Siena, Italy, in 2012. He is working toward his Ph.D. degree in the Tetrahertz (THz) Sensing Group, Department of Electrical Engineering, Mathematics and Computer Science, Delft University of Technology, The Netherlands. His research interests include analytical and numerical methods for antennas and transmission line characterization; modeling and design of THz sources based on photoconductors; and design of antennas, dielectric lens antennas, and antenna arrays. He is a Student Member of the IEEE.

Nuria Llombart (n.llombartjuan@tudelft.nl) received her M.S. and Ph.D. degrees in electrical engineering from the Polytechnic University of Valencia, Spain, in 2002 and 2006, respectively. She is an associate professor with the Tetrahertz (THz) Sensing Group, Delft University of Technology, The Netherlands. She has coauthored more than 150 journal and international conference contributions. Her research interests include the analysis and design of planar antennas, periodic structures, reflector antennas, lens antennas, and waveguide structures, with emphasis in the THz range. She was a corecipient of the H.A. Wheeler Award for the Best Applications Paper of the Year 2008 in *IEEE Transactions on Antennas and Propagation*, the 2014 THz Science and Technology Best Paper Award of the IEEE Microwave Theory and Techniques Society, and several NASA awards. She also received the 2014 IEEE Antennas and Propagation Society Lot Shafai Mid-Career Distinguished Achievement Award. She is a Senior Member of the IEEE.

Andrea Neto (A.Neto@tudelft.) received his Laurea degree in electronic engineering from the University of Florence, Italy, in 1994, and his Ph.D. degree in electromagnetics from the University of Siena, Italy, in 2000. He is a full professor of applied electromagnetism in the Department of Electrical Engineering, Mathematics and Computer Science, Delft University of Technology, The Netherlands, where he formed and leads the Tetrahertz (THz) Sensing Group. His research interests include the analysis and design of antennas, with emphasis on arrays, dielectric lens antennas, wideband antennas, electromagnetic band-gap structures, and THz antennas. He was a corecipient of the H.A. Wheeler Award for the Best Applications Paper of the Year 2008 in *IEEE Transactions on Antennas and Propagation*, the Best Innovative Paper Prize at the 30th European Space Agency Antenna Workshop in 2008, and the Best Antenna Theory Paper Prize at the European Conference on Antennas and Propagation in 2010. He is a Fellow of the IEEE.

REFERENCES

[1] K. C. Gupta, R. Garg, I. Bahl, and P. Bhartia, *Microstrip Lines and Slotlines*. Norwood, MA: Artech House, 1996.

[2] D. P. Kasilingam and D. B. Rutledge, "Surface-wave losses of coplanar transmission lines," in *Proc. 1983 IEEE MTT-S Int. Microwave Symp. Digest*, Boston, 1983, pp. 113–116.

[3] F. Mesa, D. R. Jackson, and M. J. Freire, "Evolution of leaky modes on printed circuit lines," *IEEE Trans. Microwave Theory Tech.*, vol. 50, no. 1, pp. 94–104, 2002.

[4] H. Shigesawa, M. Tsuji, and A. A. Oliner, "Simultaneous propagation of bound and leaky dominant modes on printed circuit lines a new general effect," *IEEE Trans. Microwave Theory Tech.*, vol. 43, no. 12, pp. 3007–3019, 1995.

[5] S. Bruni, N. Llombart, A. Neto, G. Gerini, and S. Maci, "Problem matched basis functions for microstrip coupled slot arrays based on transmission line Green's functions (TLGF)," *IEEE Trans. Antennas Propagat.*, vol. 53, no. 11, pp. 3556–3567, 2005.

[6] F. Mesa, C. Di Nallo, and D. R. Jackson, "The theory of surface-wave and space-wave leaky-mode excitation on microstrip lines," *IEEE Trans. Microwave Theory Tech.*, vol. 47, no. 2, pp. 207–215, 1999.

[7] F. Mesa and D. R. Jackson, "Investigation of integration paths in the spectral domain analysis of leaky modes on printed circuit lines," *IEEE Trans. Microwave Theory Tech.*, vol. 50, no. 10, pp. 2267–2275, 2002.

[8] A. Neto and S. Maci, "Green's function for an infinite slot printed between two homogeneous dielectrics. I. Magnetic currents," *IEEE Trans. Antennas Propagat*, vol. 51, no. 7, pp. 1572–1581, 2003.

[9] L. B. Felsen and Nathan Marcuvitz, *Radiation and Scattering of Waves*. New York: Wiley., 1994.

[10] J. C. Rautio, "An investigation of microstrip conductor loss," *IEEE Microwave Mag.*, vol. 1, no. 4, pp. 60–67, 2000.

[11] D. Cavallo, A. Neto, and G. Gerini, "Green's function based equivalent circuits for connected arrays in transmission and in reception," *IEEE Trans. Antennas Propagat.*, vol. 59, no. 5, pp. 1535–1545, 2011.

[12] M. Albani, A. Mazzinghi, and A. Freni, "Rigorous MoM analysis of finite conductivity effects in RLSA antennas," *IEEE Trans. Antennas Propagat.*, vol. 59, no. 11, pp. 4023–4032, 2011.

[13] F. Mesa and D. R. Jackson, "A novel approach for calculating the characteristic impedance of printed circuit lines," *IEEE Microwave Wireless Components Lett.*, vol. 15, no. 4, pp. 283–285, 2005.

[14] S. L. van Berkel, N. Lombart, and A. Neto, "Complex characteristic impedance of transmission lines at high frequencies," in *Proc. Tenth European Conf. Antennas and Propagation (EuCAP 2016)*, Davos, Switzerland, 2016, to be published.

[15] R. O'Brient, P. A. R. Ade, Z. Ahmed, R. W. Aikin, M. Amiri, S. Benton, C. Bischoff, J. J. Bock, J. A. Bonetti, J. A. Brevik, B. Burger, G. Davis, P. Day, C. D. Dowell, L. Duband, J. P. Filippini, S. Fliescher, S. R. Golwala, J. Grayson, M. Halpern, M. Hasselfield, G. Hilton, V. V. Hristov, H. Hui, K. Irwin, S. Kernasovskiy, J. M. Kovac, C. L. Kuo, E. Leitch, M. Lueker, K. Megerian, L. Moncelsi, C. B. Netterfield, H. T. Nguyen, R. W. Ogburn, IV, C. L. Pryke, C. Reintsema, J. E. Ruhl, M. C. Runyan, R. Schwarz, C. D. Sheehy, Z. Staniszewski, R. Sudiwala, G. Teply, J. E. Tolan, A. D. Turner, R. S. Tucker, A. Vieregg, D. V. Wiebe, P. Wilson, C. L. Wong, W. L. K. Wu, and K. W. Yoon, "Antenna-coupled TES bolometers for the Keck Array, Spider, and Polar-1," *Proc. SPIE*, vol. 8452, p. 84521G, Sept. 2012.

[16] P. K. Day, H. G. LeDuc, B. A. Mazin, and A. Vayonakis, and J. Zmuidzinas, "A broadband superconducting detector suitable for use in large arrays," *Nature*, vol. 425, no. 6960, pp. 817–821, 2003.

[17] S. Doyle, P. Mauskopf, J. Naylon, A. Porch, and C. Duncombe, "Lumped element kinetic inductance detectors," *J. Low Temp. Phys.*, vol. 151, no. 1–2, pp. 530–536, 2008.

[18] V. V. Schmidt, *The Physics of Superconductors: Introduction to Fundamentals and Applications*. Berlin: Springer-Verlag, 1997.

[19] A. Iacono, "Large focal plane arrays for tetrahertz imaging," Ph.D. dissertation, Dept. Elect. Eng., Technische Universiteit Eindhoven, The Netherlands, 2012.